Hydrogeology Journal (2018) 26:2507–2520
https://doi.org/10.1007/s10040-018-1789-z

PAPER

Spatial and temporal dynamics of deep percolation, lag time and recharge in an irrigated semi-arid region

F. Nazarieh[1] · H. Ansari[1] · A. N. Ziaei[1] · A. Izady[2] · K. Davari[1] · P. Brunner[3]

Received: 11 October 2017 / Accepted: 25 April 2018 / Published online: 22 May 2018

Abstract

The time required for deep percolating water to reach the water table can be considerable in areas with a thick vadose zone. Sustainable groundwater management, therefore, has to consider the spatial and temporal dynamics of groundwater recharge. The key parameters that control the lag time have been widely examined in soil physics using small-scale lysimeters and modeling studies. However, only a small number of studies have analyzed how deep-percolation rates affect groundwater recharge dynamics over large spatial scales. This study examined how the parameters influencing lag time affect groundwater recharge in a semi-arid catchment under irrigation (in northeastern Iran) using a numerical modeling approach. Flow simulations were performed by the MODFLOW-NWT code with the Vadose-Zone Flow (UZF) Package. Calibration of the groundwater model was based on data from 48 observation wells. Flow simulations showed that lag times vary from 1 to more than 100 months. A sensitivity analysis demonstrated that during drought conditions, the lag time was highly sensitive to the rate of deep percolation. The study illustrated two critical points: (1) the importance of providing estimates of the lag time as a basis for sustainable groundwater management, and (2) lag time not only depends on factors such as soil hydraulic conductivity or vadose zone depth but also depends on the deep-percolation rates and the antecedent soil-moisture condition. Therefore, estimates of the lag time have to be associated with specific percolation rates, in addition to depth to groundwater and soil properties.

Keywords Groundwater recharge · Lag time · MODFLOW-NWT · Semi-arid region · Vadose zone

Introduction

Estimation of groundwater recharge is crucial for water resources management in arid and semi-arid regions (Kinzelbach et al. 2003; Sharma and Hughes 1985; Wheater et al. 2010). Groundwater recharge is spatially and temporally variable (Brunner et al. 2004; Kinzelbach et al. 2002; Scanlon et al. 2002).

The rate of infiltration originating from precipitation or irrigation constitutes the upper boundary for groundwater recharge. Evaporation and transpiration processes close to the soil surface reduce infiltration rates (Brunner et al. 2008; Healy 2010). The difference between the amount of water involved in infiltration and that involved in evapotranspiration is equal to the amount of water for deep percolation. Deep-percolation water passes through the vadose zone and reaches the saturated zone as groundwater recharge. A considerable lag time between the start of deep percolation from root zone and groundwater recharge can occur in arid semi-arid regions (de Vries and Simmers 2002). This lag time can vary significantly, exceeding decades to centuries (Rossman et al. 2014); therefore, the consideration of lag time in recharge estimation and groundwater modeling studies can be of major importance (Hubbell et al. 2004; Turkeltaub et al. 2014).

A range of studies have analyzed these infiltration dynamics. Fluctuations in deep-percolation rate are dampened in the vadose zone and result in steady recharge rates (Dickinson

✉ H. Ansari
Ansary@um.ac.ir

[1] Water Engineering Department, College of Agriculture, Ferdowsi University of Mashhad, Mashhad, Iran

[2] Water Research Center, Sultan Qaboos University, Muscat, Oman

[3] Centre for Hydrogeology and Geothermics (CHYN), University of Neuchâtel, 2000 Neuchâtel, Switzerland

et al. 2014). Above all, the damping depth is related to the mean percolation flux and hydraulic conductivity (Corona et al. 2017); however, varying deep-percolation rates caused by episodic precipitation or irrigation can result in transient recharge (Dickinson et al. 2014). In arid or semi-arid areas, groundwater recharge is often governed by such episodic precipitation or irrigation events (Harrington et al. 2002; Pfletschinger et al. 2014), and thus transient recharge rates occur, even in areas with a thick vadose zone.

Several approaches to estimate lag time have been proposed, for example isotopic tracer methods (Cook and Solomon 1995; Horst et al. 2008), while other methods include impulse response functions (Hocking and Kelly 2016) and time series analysis (O'Reilly 2004). These techniques are not straightforward to implement and typically provide only point estimates; additionally, a range of numerical approaches has also been employed to understand infiltration processes in the vadose zone by solving the Richards equation (Brunner et al. 2012; Miller et al. 2006). The kinematic wave approximation of Richards equation is a simplified method for investigating vadose zone fluxes (Graham and Butts 2005; Hunt et al. 2008; Singh and Joseph 1994; Smith 1983). The widely used groundwater flow model MODFLOW (Harbaugh 2005) can simulate vadose zone processes (Niswonger et al. 2006) using this one-dimensional (1D) kinematic wave approximation.

Hunt et al. (2008) studied the importance of the vadose zone on recharge in a humid region. Their study results revealed the importance of vadose zone processes on infiltration and recharge dynamics. Grismer (2013) used a simple model to evaluate the lag time from agricultural deep percolation. The results of this study highlighted the importance of deep-percolation rates in lag time calculation. Cao et al. (2016) accessed the effect of increasing vadose zone thickness on recharge dynamics. Their model results indicated that the increasing thickness of the vadose zone smoothed the temporal variability of recharge, increased storage in the vadose zone, and increased the lag time between the start of deep percolation and recharge.

The main objective of this study is to assess the spatial variability of lag times in an irrigated area in Iran featuring a wide range of different depths to groundwater, soil types, land-use types and irrigation rates. The focus is on lag time because it is a good integrative proxy representing the combined effects of the vadose zone properties and antecedent conditions. The variability of all of these factors is more important than in the previously reviewed studies and leads to a significant variability of lag times in the same catchment. The study area therefore provides an unique opportunity for the evaluation of the effective factors that control the lag time such as soil hydraulic properties, the vadose zone thickness and deep-percolation rates. Based on the assessment of lag time throughout the field site, implications for water resources management are discussed.

Materials and methods

Study area

The Neishaboor plain (Fig. 1) covers an area of 4,917 km^2 and is located in the hillside of the Binalood Mountains in north-eastern Iran. The climate in this area is semi-arid according to the Köppen-Geiger system (Peel et al. 2007). The depth to groundwater ranges from 198 m in the Binalood foothills to 4 m in areas close to the main river, the Kalshour River. Average annual precipitation is 265 mm, ranging from 180 mm in dry years to 360 mm in wet years. The mean annual temperatures in the mountainous and the plain areas are 13 and 13.8 °C, respectively. The potential annual evapotranspiration in the study area is between 2,040 and 2,760 mm/year. Regional groundwater flow originates from Binalood hillside (east and northeast) and also Rokh plain (south) and discharges to the southwest (Fig. 1). Recharge from lateral subsurface flow is estimated to range from 10 to 14 mm/year (Izady et al. 2015).

The Neishaboor aquifer is unconfined. During the past few decades, severe overexploitation of this aquifer has resulted in a decrease of the water table of 1 m/year. A further increase in groundwater extraction in this plain has been prohibited since 1986 (Khorasan Razavi Regional Water Authority 2011). Groundwater resource depletion resulted in adverse environmental impacts such as increased energy cost for groundwater abstraction, a decrease in groundwater quality and land subsidence (Nameghi et al. 2014).

The agricultural sector is the largest consumer of groundwater resources in the Neishaboor plain; 90% of exploited groundwater is used for agriculture. Irrigation efficiency was reported to be approximately 40% for the study area (Khorasan-Razavi Regional Water Authority 2010); thus, one of the main sources of groundwater recharge is irrigation return flow. The average amount of recharge (from precipitation and irrigation return flows) is about 176 mm/year (Izady et al. 2015).

A geoelectrical survey using the electrical resistivity method (Zharf Poya 2016) identified one main aquifer layer in the study area. This survey included 646 vertical electrical sounding (VES) surveys on 31 profiles, where the profiles were approximately in the southwest to the northeast direction on parallel lines. An example of a geoelectrical cross section of the study area is presented in (Fig. 2c). Based on the geoelectrical cross-sections (Fig. 2a), 24 zones of hydraulic conductivity (K) and specific yield (Sy; Fig. 2b) could be identified. Gradual changes of electrical resistivity indicate relative uniformity of the recent alluvial deposits, alluvial terraces and bedrock. The piedmont and marginal areas are composed of coarse alluvial sediments, diluvium with a substantial groundwater storage capacity and Neogene marl bedrock. Other areas in the plain are composed of materials with

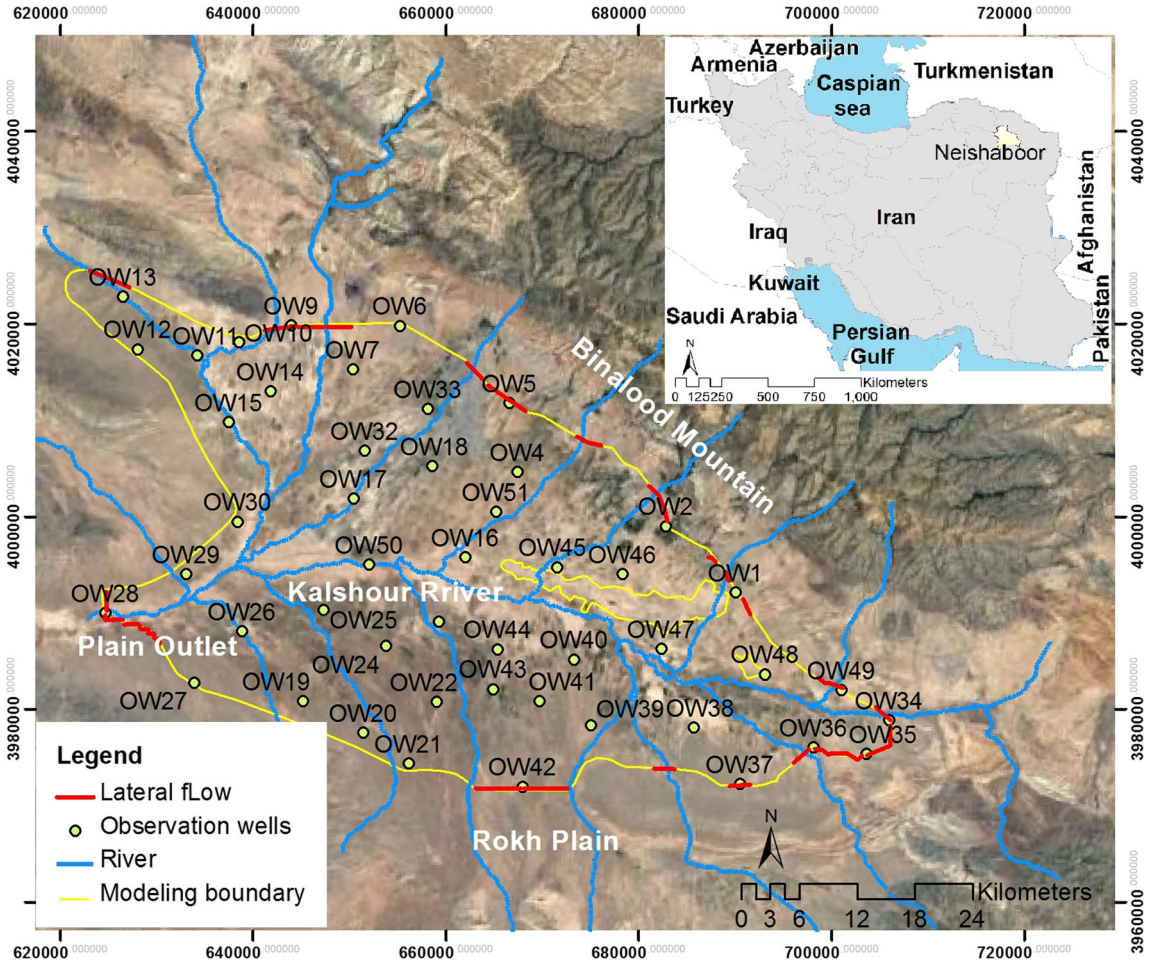

Fig. 1 Neishaboor Plain (Landsat Image), major rivers, observation wells, and lateral flow boundaries

finer textures, consisting of Neogene marl and andesite bedrock (Zharf Poya 2016).

The vadose zone soil-texture map is represented in Fig. 3. This map was elaborated on the basis of the available data including the geoelectric cross-sections, drilling logs and geological maps. Loamy sand is the dominant soil in the marginal areas while in the central parts mainly sandy loam and loam soils are present. Other soil textures include sandy clay loam and clay loam, around the main rivers and sparsely sandy soil textures.

Numerical simulator

The Newton formulation of a finite-difference groundwater flow model (MODFLOW-NWT), which was developed by Niswonger et al. (2011), was applied for saturated zone modeling. The UZF package was utilized to simulate flow in the vadose zone. It is based on the Kinematic-wave approximation of the Richards equation (Niswonger et al. 2006):

$$\frac{\partial\theta}{\partial t}+\frac{\partial K(\theta)}{\partial z}+i=0 \tag{1}$$

where θ is volumetric water content (m^3/m^3), t is time (d), $K(\theta)$ is the unsaturated hydraulic conductivity (m/day), z is the elevation in the vertical direction (m), i is evapotranspiration rate per unit depth (m/day/m). The unsaturated hydraulic conductivity is calculated using the Brooks-Corey function (Niswonger et al. 2006):

$$K(\theta)=K_s\left(\frac{\theta-\theta_r}{\theta_s-\theta_r}\right)^{\varepsilon} \tag{2}$$

where K_s is the saturated hydraulic conductivity (m/day), ε is Brooks-Corey exponent (−), θ_s is saturated water content (m^3/m^3) and θ_r is residual water content (m^3/m^3). The amount of residual water content is calculated based on the difference between saturated water content θ_s and specific yield Sy (m^3/m^3; Niswonger et al. 2006).

The velocity of the deepest point along a trailing wave is calculated by Eq. (3) in the UZF package (Niswonger et al. 2006):

$$v(\theta)=\frac{\varepsilon K_s}{Sy}\left[\frac{\theta-\theta_r}{Sy}\right]^{\varepsilon-1} \tag{3}$$

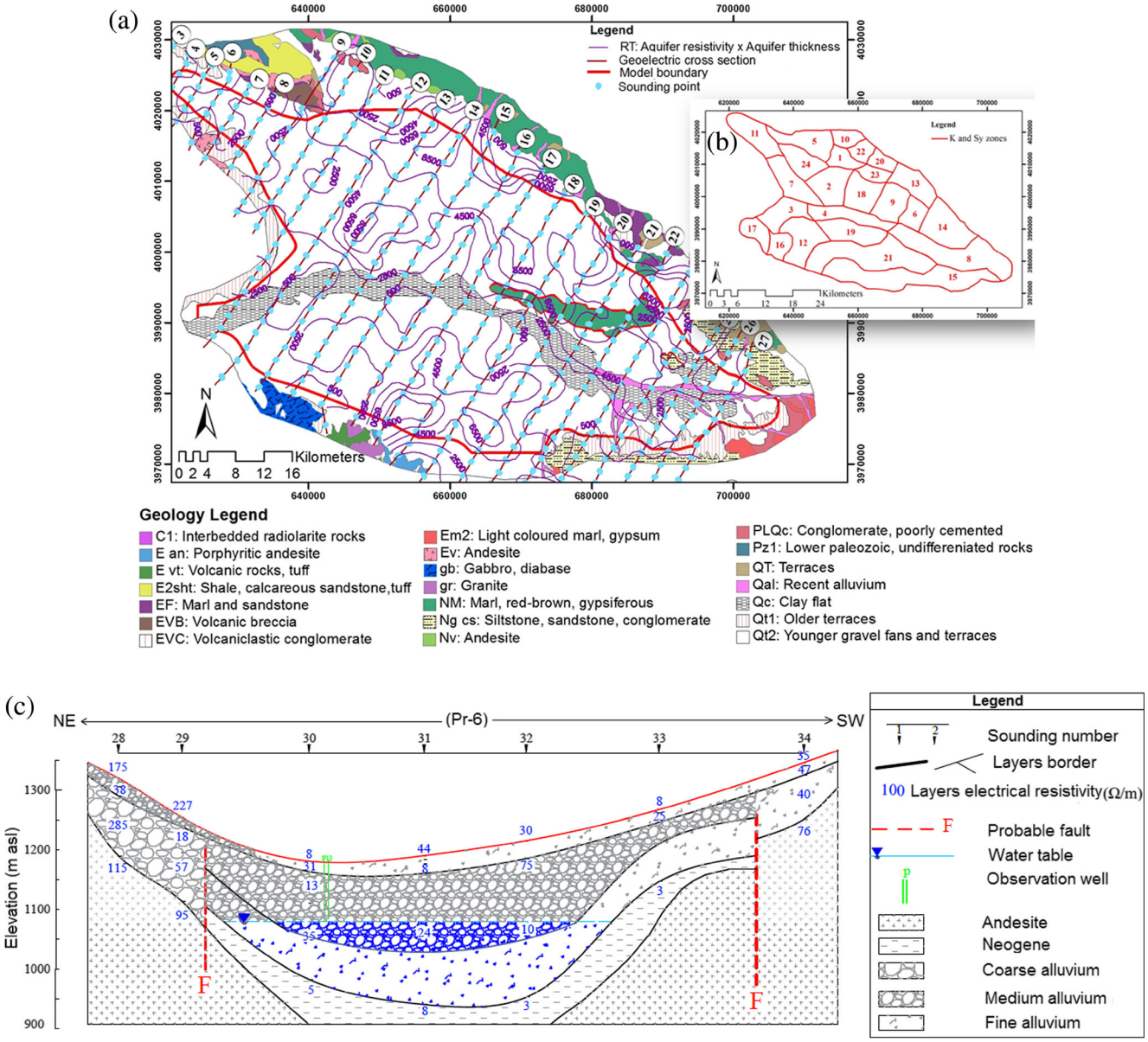

Fig. 2 **a** Geological map of the Neishaboor plain (Zharf Poya 2016), **b** hydraulic conductivity (*K*) and specific yield zones, and **c** the geoelectric cross section no. 6

where $\nu(\theta)$ and θ are the vertical velocity (m/day) and water content at the deepest point along a trailing wave. In the current study, the lag time is calculated for the wetting front in a month with the highest water content. Based on the calculated velocity of the trailing wave in UZF, lag time was calculated for the maximum water content wave as Eq. (4):

$$\mathrm{Lag}_t = \frac{D_m}{\nu(\theta)} \tag{4}$$

where D_m is the mean depth to water table (m).

Model setup

The groundwater model was set up using a single layer and 500 × 500 m cell size. The data layers utilized for model setup included a digital elevation model (SRTM 90 m DEMs), bedrock elevation, plain boundary, geology map, time series of hydraulic heads at 48 observation wells and mean monthly pumping rates from 1,830 exploitation wells. The pumping rates were adapted from Izady et al. (2014, 2015). Based on the digital elevation model, bedrock elevation and hydraulic heads at observation wells, estimates of bedrock depth vary between 0 and 250 m, and the thickness of saturated zone is between 0 to 194 m.

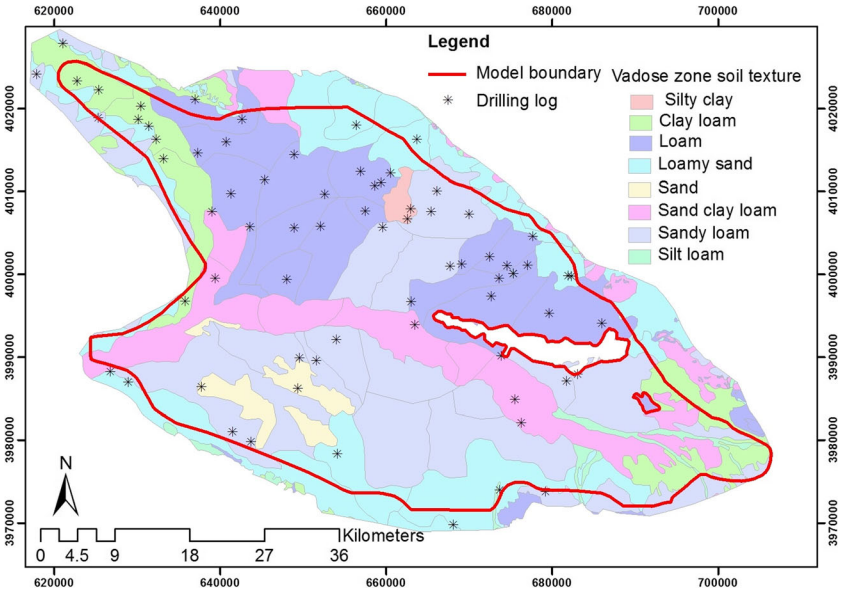

Fig. 3 Neishaboor vadose zone soil texture, and location of drilling logs

Several types of boundary conditions were implemented. These include lateral subsurface flow, groundwater abstraction through pumping wells, and deep-percolation rates through the vadose zone. The packages used for simulating these boundary conditions include CHD, WELL and UZF respectively. These packages are documented in MODFLOW manual (Harbaugh 2005). The model was run with daily time units and monthly stress periods.

Lateral subsurface flows in the alluvial fans were specified based on the geological map, the topography, and river branches (Fig. 1). They were simulated using constant head boundary conditions. These boundary conditions were based on the observed monthly hydraulic heads situated at the model boundaries. Abstraction rates from pumping wells were based on the abstraction rates of 2 years (1999–2009). A linear rate of change for abstraction rates in this period was assumed (Izady et al. 2015).

The upper boundary condition of the vadose zone is equal to the amount of water that leaves the root zone (constitute deep percolation). The spatiotemporal distribution of these percolation rates are based on a previous study by Izady et al. (2015) who elaborated a SWAT model for this region. This model simulated the daily water balance, considering the spatial distribution of land use, soil textures, irrigation, rainfall patterns and potential evaporation rates. The distributed, mean monthly deep-percolation rates from SWAT were implemented in MODFLOW at each stress period.

The Brooks-Corey coefficients were defined in two steps. First, the relations between the Brooks-Corey coefficients and soil texture were determined, based on values proposed by Rawls et al. (1982). Then, based on a vadose zone soil texture map (Fig. 3), Brooks-Corey parameters were assigned to each soil texture.

Soil texture and mean deep-percolation rate affect the initial water content. The soil-water content map was elaborated based on overlapping vadose-zone-soil texture and the deep-percolation-rate-polygons map. The water content at first was set equal to the residual water content at each polygon with regard to the soil texture. Then, before calibration of other parameters, the model was run several times for Oct. 1999 to Sep. 2000 (warm-up period) to get better estimation for initial water content. The model was run repeatedly until it had steady-state water balance in the vadose zone and stable water table.

Sensitivity analysis and model calibration

The composite-scaled sensitivity analysis was performed before the calibration procedure to evaluate the relative importance of model parameters on the water-table fluctuation. Furthermore, it is important to know whether the model sensitivity in the entire range of parameters is the same or whether it will change for a different range of the parameters. In order to investigate this matter, parameters related to the soil texture were explored for three types of soil texture: coarse, medium and fine. Also, according to the deep percolation obtained from SWAT model, three different zones associated with deep percolation were distinguished: non-irrigated, irrigated and heavily irrigated regions. Average annual deep-percolation rates at each zone were used used for sensitivity analysis**.** Finally, a total of 21 parameters were used for the sensitivity analysis (see Table 1).

Parameter sensitivity analysis was accomplished by parameter estimation code PEST (Doherty 2016) and with 1% perturbations of the parameters. The sensitivity analysis was performed on a 12-year period (Oct. 2000–Sep. 2012) using 6,770 head measurements from 48 observation wells**.**

As mentioned earlier, the simulation period was 12 years; 10 years (Oct. 2000– Sep. 2010) was chosen for calibration and 2 years (from Oct. 2010 to Sep. 2012) for validation. The water-table elevation was initialized by defining the water table at

Table 1 Parameters values used in the sensitivity analysis

Parameter	Unit	Type	Symbol (Fig. 4)	Starting value	Lower bound	Upper bound
Hydraulic conductivity (K)	[m/day]	Coarse	K-C	20	15	100
		Medium	K-M	8	1	16
		Fine	K-F	1	0.1	1.5
Specific yield (Sy)	[m^3/m^3]	Coarse	Sy-C	0.21	0.2	0.35
		Medium	Sy-M	0.1	0.12	0.23
		Fine	Sy-F	0.05	0.01	0.15
Saturated vertical hydraulic conductivity (K_S)	[m/day]	Coarse	K_S-C	3	2	20
		Medium	K_S-M	2	0.4	2.5
		Fine	K_S-F	0.4	0.06	0.6
Brooks-Corey epsilon (ε)	[−]	Coarse	ε-C	3.5	3	6
		Medium	ε-M	4.5	4	8
		Fine	ε-F	7.5	7	12
Saturated water content of vadose zone (θ_s)	[m^3/m^3]	Coarse	θ_s-C	0.36	0.351	0.50
		Medium	θ_s-M	0.4	0.35	0.55
		Fine	θ_s-F	0.45	0.4	0.58
Initial water content of vadose zone (θ_i)	[m^3/m^3]	Coarse	θ_i-C	0.151	0.1	0.50
		Medium	θ_i-M	0.301	0.3	0.55
		Fine	θ_i-F	0.401	0.27	0.58
Deep-percolation rate (FINF)	[m/day]	Non-irrigated	D-N-Irr	0.0006	0.0001	0.0008
		Irrigated	D-Irr	0.0003	0.0001	0.0008
		Heavily irrigated	D-H-Irr	0.00015	0.00001	0.0008

an observation well as a constant head boundary for the Oct. 1999–Sep. 2000 period. Model parameters were calibrated manually until the water table and water balance component in the vadose zone and saturated zone got close to the Neishaboor plain water-balance values published by Ahmadi et al. (2012) and Izady et al. (2015). Following the manual calibration, the most sensitive parameters of the model were calibrated automatically by inverse modeling using PEST software. The model parameters were calibrated by minimizing the difference between simulated and observed water tables in 48 observation wells (Fig. 1). The calibrated model was evaluated by the mean absolute error (MAE), mean bias error (MBE), root mean square error (RMSE), and normalized RMSE (NRMSE). The NRMSE at each observation well was obtained by dividing RMSE by the difference between maximum and minimum observed water-table elevation.

Results and discussion

Water-table sensitivity analysis

Results of the composite scaled sensitivity (CSS) analysis are shown in Fig. 4. The values of CSS in this figure revealed that

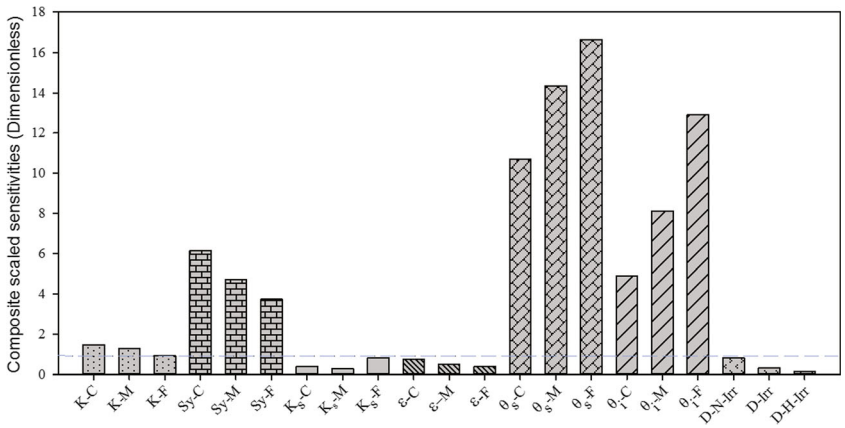

Fig. 4 Composite-scaled parameter sensitivities calculated by PEST using head data of observation wells

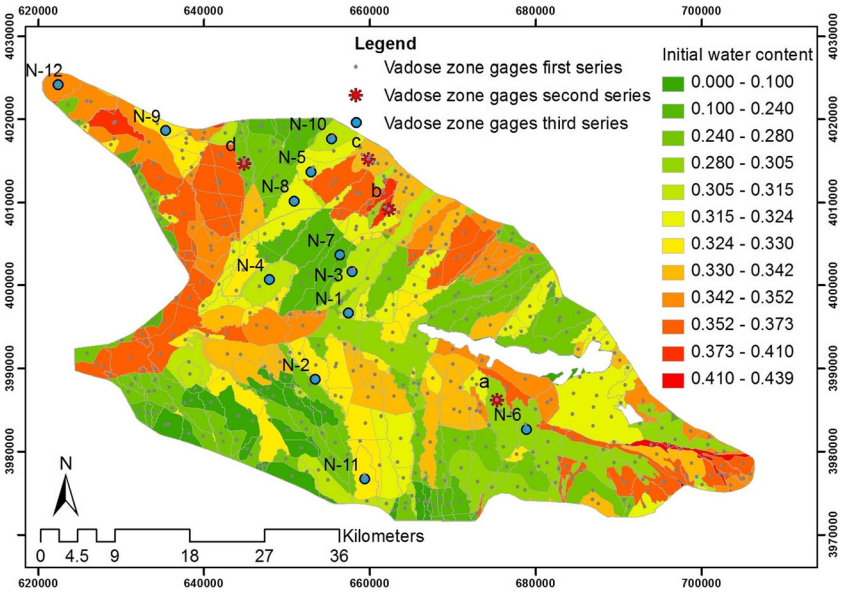

Fig. 5 Initial water content map and vadose zone gages

the sensitivity of the water-table elevation to saturated water content (θ_s) and the initial water content of the vadose zone (θ_i) was significant. Cao (2011) also noted that the actual recharge is very sensitive to a decrease in θ_s and an increase in θ_i. *Sy* was the third most sensitive parameter. Note that *Sy* is used by MODFLOW in both the vadose zone and saturated zone simulations.

Figure 4 illustrates that the water-table fluctuations were more sensitive to saturated zone parameters (*K* and *Sy*) in areas with coarse textured soils. However, the most sensitive parameters in the vadose zone (θ_s and θ_i) are related to the finer soil textures. It should be noted that finer textured soils have higher residual water contents; thus, variations in the parameters that control soil water content in the finer textured soils lead to more changes in the amount of deep percolation and consequently water-table fluctuations.

CSS values lower than 1.0 indicate that the sensitivity contribution is less than the effect of observation error and these parameters are more likely to be poorly estimated (Hill 1998). Therefore, only four parameters with CSS values greater than 1.0, namely *K*, *Sy*, θ_s and θ_i (see Fig. 4), were utilized for calibration, and other parameter values were kept fixed. The calibrated zones for *K* and *Sy* are presented in Fig. 2b and zones used for θ_s and θ_i, are shown in Figs. 3 and 5 respectively.

Since the model showed significant sensitivity to the initial water content, the initial water content was optimized by running the model from Oct. 1999 to Sep. 2000 (warm-up period) before calibrating. The model was run for this period several times. For these model runs, an initial guess of the calibration parameters was used. The model was run for the aforementioned period until no significant changes (smaller than 10%) in the amount of water stored in the vadose zone were observed. To check this, 400 samples cells were chosen. These sample cells are located at the center of the water content map polygons shown in Fig. 5 (as the first series of vadose zone gages). After these initial runs, the mean difference between simulated and observed water-table elevation in the aquifer was also determined. Difference amounted to 0.5 m for this period (1 year) suggesting that the initial guess of the parameters was acceptable. This initial water content values were subsequently used in the transient calibration described in the upcoming section. The initial water content obtained in this procedure is shown in Fig. 5.

Calibrated groundwater model

Table 2 gives the model performance statistics for calibration (10 years) and validation period (2 years). Given that the difference between the maximum and minimum water-table elevation of the Neishaboor plain is about 160 m, the value of MAE, MBE, RMSE and NRMSE (Table 2) can be considered satisfactory. MAE and RMS are performance statistics to calculate the magnitude of the average error and MBE is a measure of the average model bias, while the negative MBE

Table 2 Model performance statistics for the calibration and validation periods

Simulation period	MAE (m)	MBE (m)	RMSE (m)	SDV RMSE[a]	NRMSE (%)
Calibration	1.34	−0.64	1.52	1.11	17.5
Validation	1.53	−0.49	1.62	1.50	56.3

[a] Standard deviation of RMSE at all observation wells

values illustrate that there is a small underestimation in the simulated values.

In order to visualize model performance in time, the comparison of observed and simulated water-table fluctuations is shown in Fig. 6a where the area-weighted average values of the water-table elevation at observation wells are plotted. The observed and simulated water-table contour lines are represented in Fig. 6b. Overall, in the calibration period, RMSE in 46% of observation wells was less than 1 m, in 35% of wells it was between 1 and 2 m and in 19% of wells, it was more than 2 m. These values during the validation period were 43, 33, and 24%, respectively. These values of RMSE were acceptable regarding the number of observation wells, the model resolution, the accuracy of water-table data, and the scale of the study area.

The water balance components for both the vadose zone and saturated zone for 12 years of the simulation are shown in Table 3. Groundwater recharge rates (Table 3) agree with the range of mean annual recharge of 228–390 million cubic meters (MCM) reported by Ahmadi et al. (2012) and Izady et al. (2015). The average annual water balance in the saturated zone reveals that this area has a negative water balance (−226 MCM/year) while storage of water in the vadose zone increases (28 MCM/year) annually. A rising storage of water in the vadose zone is related to the decline of the water table. The water-table decline increases the extent of the vadose

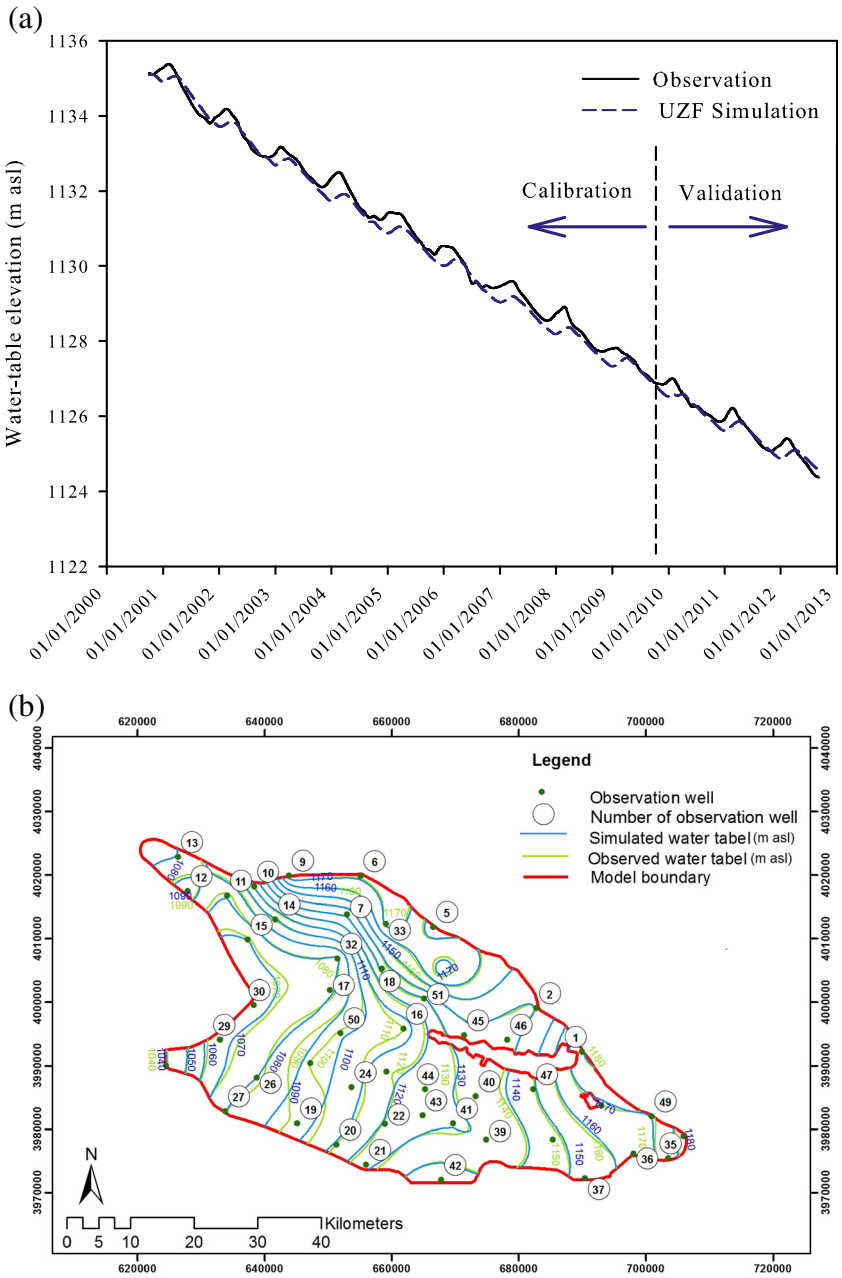

Fig. 6 **a** Observed and simulated water-table fluctuations of Neishaboor plain, **b** Observed and simulated water-table contour lines at the last time step (September 2012)

Table 3 Annual water balance in the vadose and saturated zones (MCM)

Water year	Vadose zone			Saturated zone				
	In	Out	Storage change	In		Out		Storage change
	Deep percolation	Recharge		Recharge	Boundary	Well	Boundary	
2000–2001	376	345	31	345	50	680	45	−330
2001–2002	391	354	37	354	52	672	32	−297
2002–2003	399	356	43	356	69	663	26	−264
2003–2004	406	369	37	369	77	656	27	−237
2004–2005	419	387	32	387	79	645	28	−207
2005–2006	393	367	26	367	70	636	31	−229
2006–2007	420	380	40	380	76	626	30	−199
2007–2008	397	376	21	376	71	617	32	−202
2008–2009	405	386	20	386	68	610	35	−190
2009–2010	408	390	18	390	61	611	40	−200
2010–2011	403	392	11	392	58	611	40	−201
2011–2012	395	375	20	375	55	547	37	−154
Average	401	373	28	373	66	631	34	−226

zone. Additionally, at some points, the rate of water-table decline is more than the Darcy velocity in the vadose zone, which in some areas prevents infiltrating water from reaching the saturated zone. The flow processes in the vadose zone are described in more detail in section 'Flow in the vadose zone'.

Flow in the vadose zone

In order to illustrate the effects of the vadose zone on the temporal dynamics of recharge, the differences between monthly rates of deep percolation and simulated recharge at four representative cells (second series of vadose zone gages in Fig. 5) are shown in Fig. 7. The four cells were chosen to represent different types of deep-percolation regimes in the Neishaboor plain. The selected cells cover distinct soil textures, vadose zone thicknesses and deep-percolation rates. The soil textures at these cells consisted of sandy clay loam (Fig. 7a), silty clay (Fig. 7b), loam sand (Fig. 7c) and loam (Fig. 7d). The vadose zone thickness related to the mentioned soil textures were 19, 27, 72 and 35 m, respectively. The dark blue line in Fig. 7 shows the deep-percolation depth applied at the top of the vadose zone and the red one represents the recharge at the water table after flow through the vadose zone.

It can be inferred from Fig. 7 that, as a result of the vadose zone, the recharge dynamics did not correspond to deep percolation, both in time and magnitude. This is because a wetting front gradually spreads in the extended vadose zone and in some cases joins or overtakes other wetting fronts. Figure 7 also highlights the effects of deep percolation on the lag time. The comparison of Fig. 7a,c revealed that, although the cell of Fig. 7c had a relatively thick vadose zone (72 m) in comparison to the cell of Fig. 6a (19 m), it had less lag time (6.5 months versus 8 months) due to the larger amount of deep percolation.

The cell represented in Fig. 7a is located in the central area of the plain, where recharge from irrigation return flow is dominant. Figure 7b,c shows cells around the alluvial fans boundary with irrigated farms that receive high amounts of recharge from irrigation return flows and lateral flows of the Binalood Mountains. It can be seen in Fig. 7d that the percolated water, which originated from precipitation, has not reached the water table, even after 12 years of simulation time.

In an attempt to achieve a spatial distribution of the lag time for the entire area, vadose zone flow processes were investigated at more than 400 model grid cells (first series of vadose zone gages in Fig. 5). These cells were selected from different locations with various soil textures, vadose zone thicknesses, and model input fluxes. Table 4 shows 12 sample of these cells with annual deep percolation ranging from 29 to 168 mm/year. The locations of the 12 sample cells are shown in Fig. 5 as the third series of vadose zone gages.

As can be seen in Table 4, increasing thickness of vadose zone significantly increases the residence time of deep-percolation water in the vadose zone. For instance, in two sandy loam sample cells with an identical deep-percolation rate of 139 mm/year (cells N-1 and N-3), lag time increased from 1.3 to 5.6 months as the vadose zone thickness increased from 4.9 to 21.4 m.

Table 4 shows the effect of deep-percolation rates on lag time as well—for example, within a loam soil with vadose zone depth of about 25 m (cells N-4 and N-5), when annual deep percolation decreased from 147 to 88 mm/year, 4.3 months were added to the lag time. Other examples for

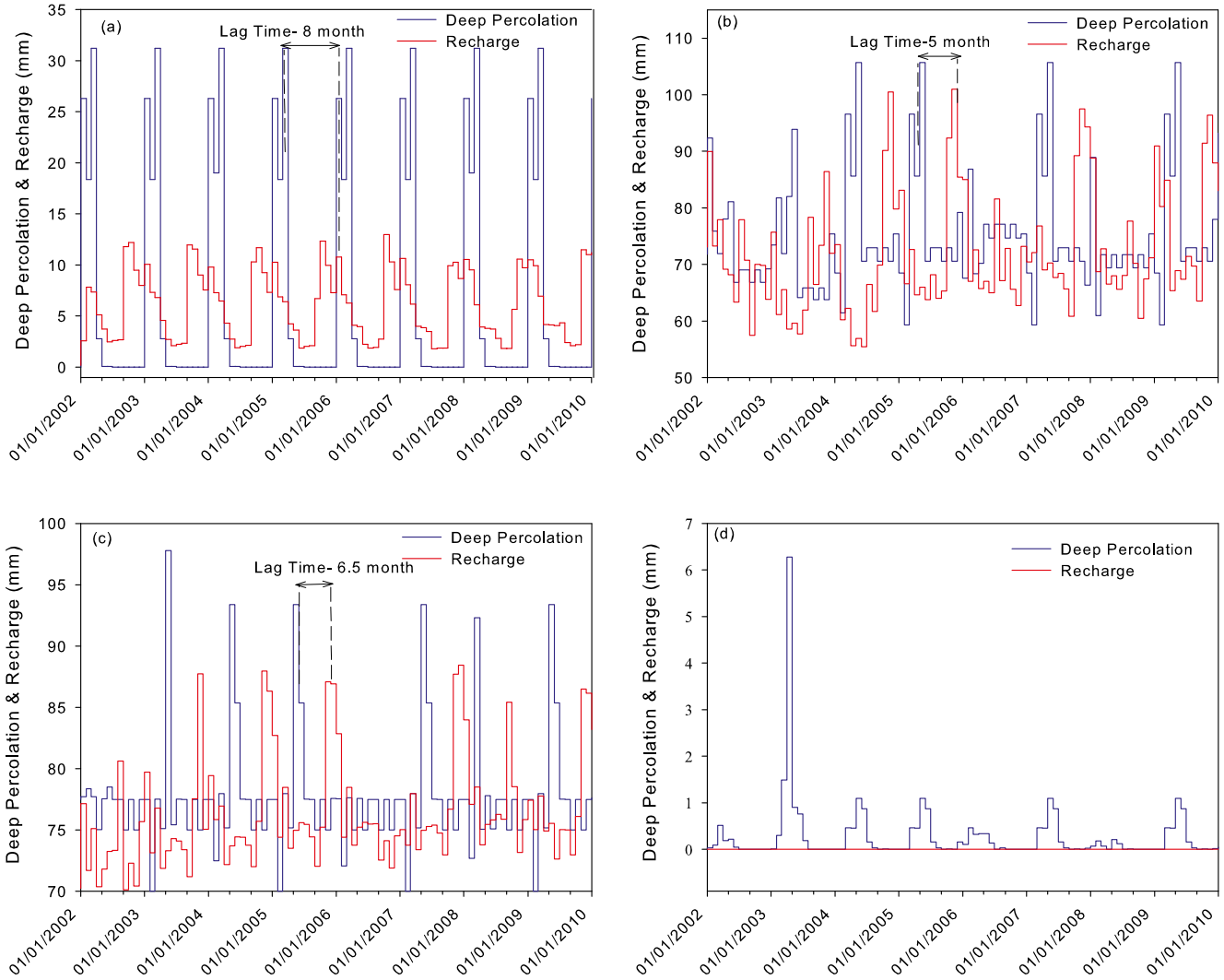

Fig. 7 Comparison of the lag times between the start of deep percolation and recharge at the water table for four sample cells: **a** sandy clay loam, **b** silty clay, **c** sandy loam and **d** loam soil texture

Table 4 Lag time with regard to soil texture, vadose zone depth and deep-=percolation rate

Cell name	Soil texture	Vadose zone depth (m)	Deep percolation (mm/year)	Lag time (months)
N-1	Sandy loam	4.9	139	1.3
N-2	Sandy loam	9.3	120	2.6
N-3	Sandy loam	21.4	139	5.6
N-4	Loam	25.0	147	7.9
N-5	Loam	25.6	88	12.2
N-6	Sandy clay loam	32.0	175	8.5
N-7	Loam	35.5	29	27.0
N-8	Loam	35.7	45	24.0
N-9	Loam	40.7	152	15.8
N-10	Loamy sand	66.8	88	35.3
N-11	Sandy loam	89.8	168	29.6
N-12	Clay loam	133.5	136	59.2

this case were cells N-7 and N-8 with about 35.5-m vadose zone thicknesses. Decreasing lag time by increasing deep percolation is related to the relation between hydraulic conductivity and water content. According to the Brooks-Corey equation, which states the function between hydraulic conductivity and water content, increasing water content in the vadose zone result in increased unsaturated hydraulic conductivity.

Since lag time changes with variation of deep percolation, it is essential to address the amount of deep percolation when presenting lag time for any specific location. Grismer (2013) also emphasized the effect of agricultural deep-percolation rates on lag time for different vegetation types. The spatial distribution of lag time in the Neishaboor plain is depicted in Fig. 8 considering vadose zone thickness and deep-percolation rate.

Figure 8 shows a considerable spatial variation of lag time in the Neishaboor plain. This variation is due to the intense irrigation in some areas of the plain (Fig. 8b) and highly variable

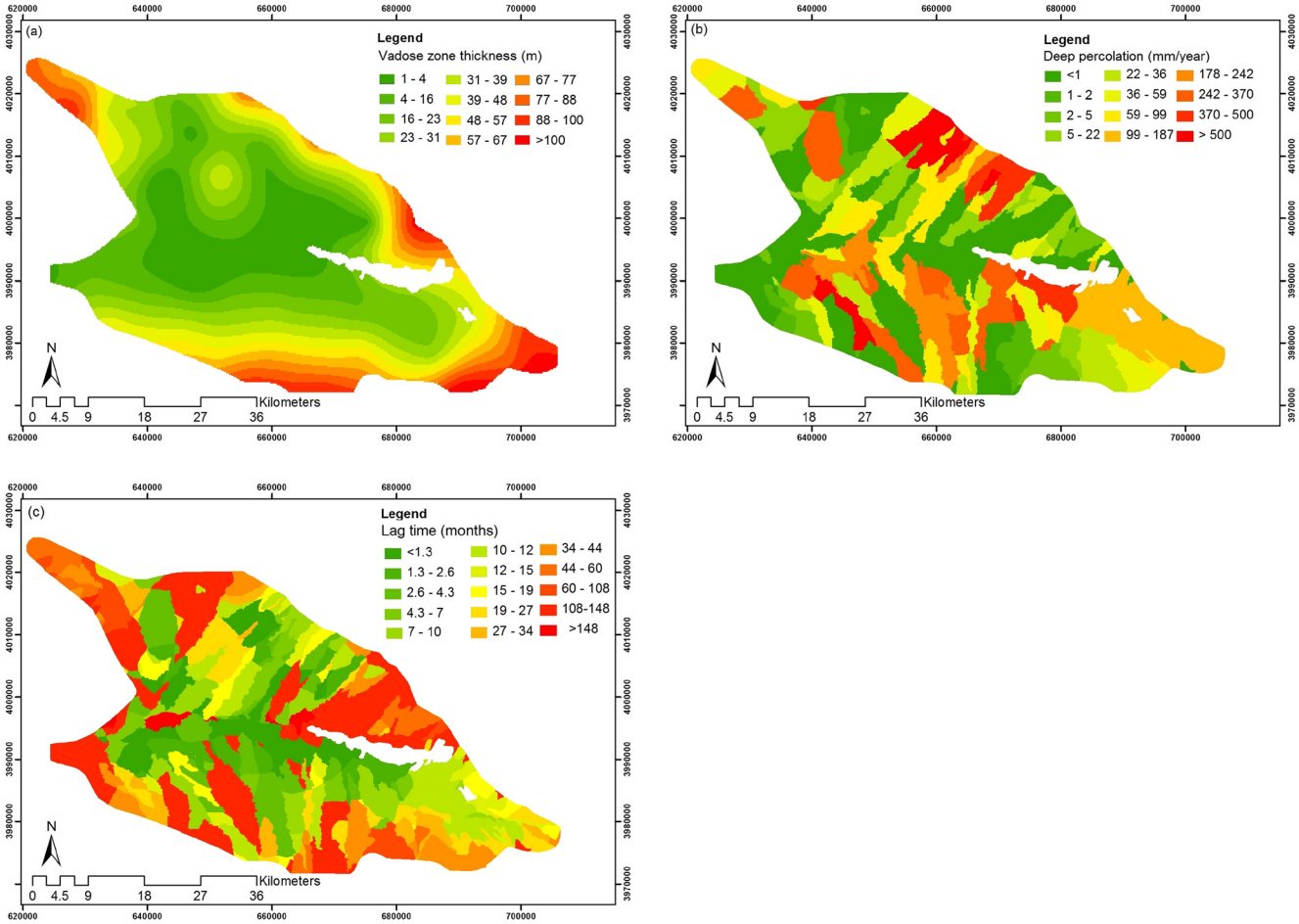

Fig. 8 Representation of **a** vadose zone thickness, **b** annual deep-percolation rate, and **c** distribution of lag time

vadose zone thickness (Fig. 8a). This figure demonstrates that spatial distribution of the recharge dynamics in the vadose zone is highly affected by the annual rate of deep percolation (Fig. 8b) and to a smaller extent by the vadose zone thickness (Fig. 8a) or soil texture (Fig. 3a)—for instance, in marginal areas of the south and south-eastern part of the plain, vadose zone thicknesses are similar (100-m vadose zone thickness) and soil texture at the south-eastern part is finer than in the south (clay loam versus loamy sand, Fig. 3). However, as a result of increased deep-percolation rates in the south-eastern part, the lag time was much less than in the southern area.

Percolation dynamics change during the flow through the vadose zone. The larger the lag time between percolation and recharge, the greater its impact on temporal variation of recharge. The effect of the vadose zone on recharge dynamics is represented by the spatial distribution of lag time in Fig. 8c. According to this figure, the calculated lag time in 40% of the plain was less than 1 year, while in 35% it was between 1 and 5 years, in 5% it was between 5 and 12 years, and in 20% of the plain it was more than 12 years.

Since the most important parameters which affect recharge dynamics are not constant in time, it is useful to draw lag-time contour lines with regard to vadose zone thickness and deep percolation. Figure 9 displays how the lag times vary with respect to vadose zone thickness and the average annual deep-percolation rate for dominant soil textures (see Fig. 3). The amount of deep percolation has an effect on the general vadose zone water content.

In general, for a given vadose zone depth, increasing deep-percolation rates cause the lag times to decrease until the soil gets saturated and therefore the the unsaturated hydraulic conductivity becomes equal with the saturated soil hydraulic conductivity. For the range of deep-percolation rates represented in Fig. 9, the lag-time changes by increasing vadose zone thickness at the contour lines related to the loam soil is slightly more than the lag-time changes related to the sandy loam soil. This is due to the smaller hydraulic conductivity in loam soils compared to sandy loam for a given deep-percolation rate. The effect of

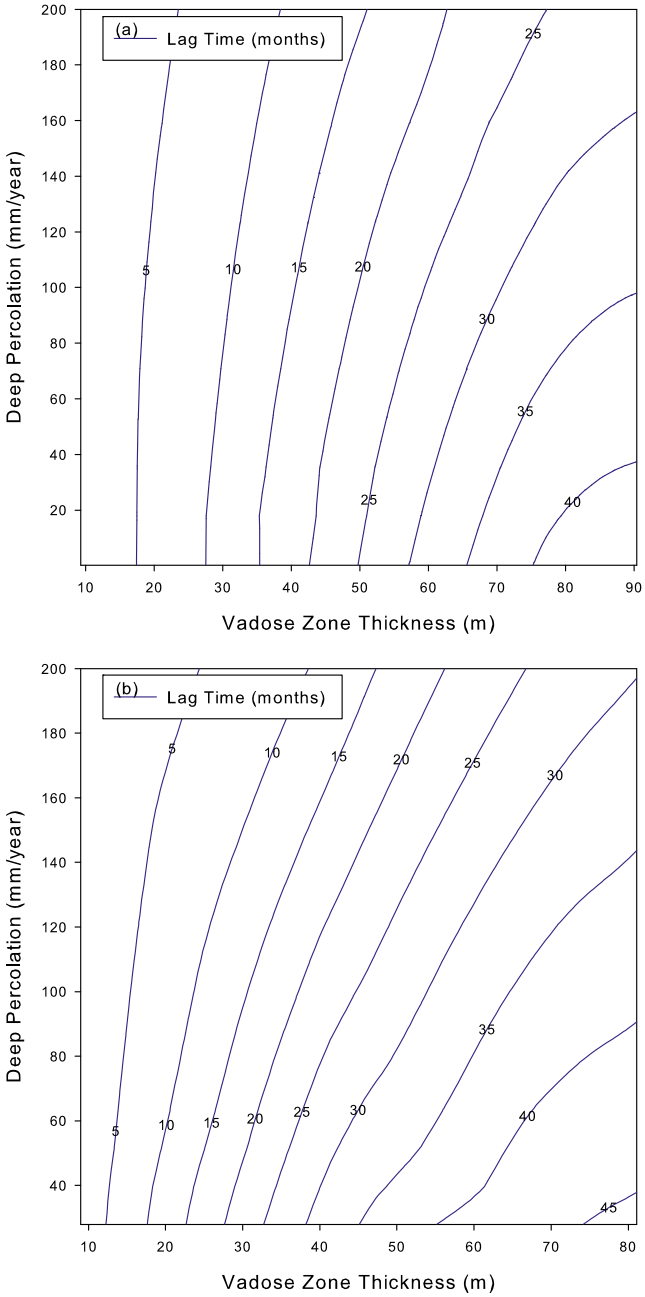

Fig. 9 Lag-time contour lines with regard to the deep-percolation rates and vadose zone thickness: **a** sandy loam soil, **b** loam soil

lower hydraulic conductivity becomes more pronounced in the thicker vadose zone.

Lag-time sensitivity analysis

The role of deep-percolation rate in the spatial dynamics of recharge was discussed in the previous section. Here the sensitivity of the temporal dynamics of groundwater recharge under various percolation regimes is investigated. Three scenarios for annual deep percolation were chosen and the model was run for each scenario. The mean annual deep-percolation rates for these three scenarios were 19, 76, and 168 mm, to represent non-irrigated, irrigated and heavily irrigated conditions respectively. These scenarios were applied for two different locations in which their vadose zone thicknesses were the same (30 m). One of these locations consisted of sandy loam soil, while the other one featured loam soil texture. The initial water content for both soil textures was defined regarding the residual water content. The amount of deep percolation for each scenario was changed by ±10, ±20, ±30 and ±40% and then lag time changes from its basic value were calculated. Figure 10 shows the sensitivity of the lag time to the deep-percolation rates under nonirrigated, irrigated and heavily irrigated condition (scenarios 1–3).

As can be seen in Fig. 10, the lag-time variation in a loam soil had a wider range with respect to the sandy loam soil (-15 -25 versus -4 -10). It revealed that the lag time was more sensitive to the amount of deep percolation in loam soil. The latter event was mainly associated with the different physical properties of loam and sandy loam soil textures.

Scenario 1 in Fig. 10 had the steepest slope in comparison to the other scenarios. It demonstrates that lag time had the higher sensitivity to changes in deep percolation under

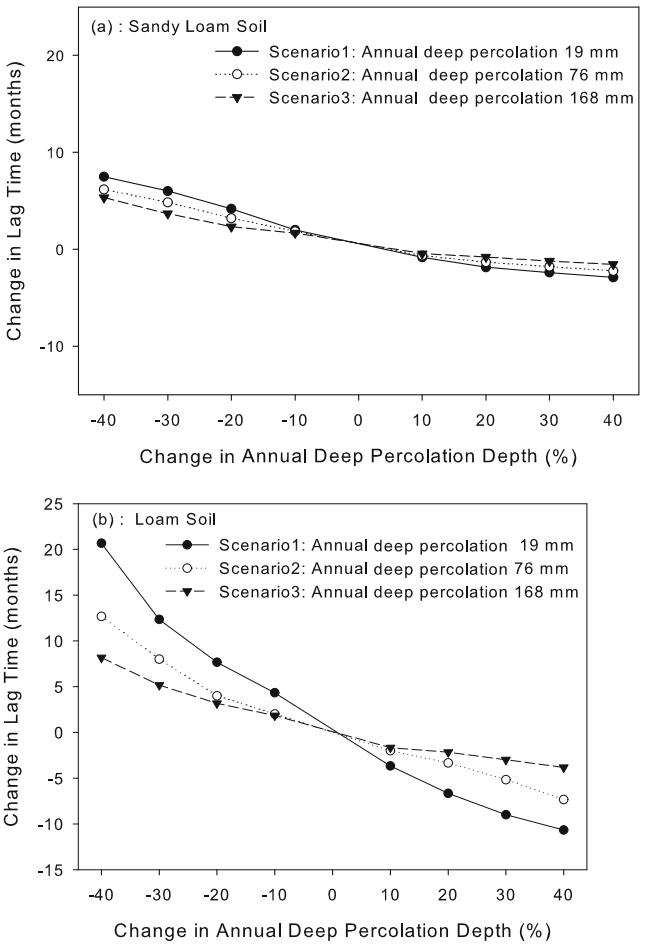

Fig. 10 The effects of changes in deep percolation (INFI) on lag time of study area: **a** sandy loam soil, **b** loam soil

nonirrigated conditions (scenario 1). The sensitivity of lag time in this condition is related to the relationship between water content and hydraulic conductivity or pressure head. The function between water content and unsaturated hydraulic conductivity or the function between water content and pressure head at the lower amount of water content have steeper slope. Therefore, under conditions of lower water content, the unsaturated hydraulic conductivity and pressure head respond more intensively to changes in water content.

According to Fig. 10, the lag time changes response to decrease and increase of the deep-percolation rate was not the same for all scenarios. In terms of decrease in deep-percolation values, the lag-time values were relatively sensitive, in comparison to the situations where deep percolation increased—for example, for loam soil in scenario 1, a 40% decrease in deep-percolation rate led to an 8-month increase in lag time, whereas a 40% increase in deep percolation resulted in only 2-month lag-time decrease.

The significant result of lag time sensitivity analysis is that in nonirrigated conditions, lag time is more sensitive to changes in deep percolation. This sensitivity is more considerable for finer soil textures; therefore, modification to irrigation management practices, especially changes from surface irrigation to pressurized irrigation, in plains like Neishaboor, affects groundwater recharge dynamics significantly.

Conclusions

The MODFLOW-NWT code and the UZF package combined with a watershed model were used for simulating the vadose and saturated zones in an agricultural area with vastly different values of depth to groundwater, soil types and irrigation regimes. The calibrated model was employed to investigate deep percolation through the vadose zone and estimate its effect on recharge dynamics. In alignment with previous studies, it is clear that that vadose zone has a significant effect on recharge dynamics.

The major factors which affect lag time in areas with high rates of deep percolation are, soil type and vadose zone thickness, while in areas with low rate of deep percolation, the lag time is dominantly affected by the deep-percolation rate. Given the importance of the deep-percolation rate, it is important to use a sufficiently fine temporal resolution to simulate these dynamics. If, for example, average annual values for deep-percolation rate are employed rather than monthly values, the estimated lag times will be biased, especially in areas with low percolation rates.

The results suggest that estimates of groundwater recharge have to be complemented with estimates of lag times under different irrigation conditions. Such information is important to large-scale groundwater management. The lag-time contour lines proposed here are helpful in illustrating the effect of different land use groundwater, groundwater management schemes and cropping patterns; thus, it is suggested that the approach is also applicable to other areas.

Acknowledgements The authors would like to acknowledge the financial support from the Ministry of Science, Research and Technology of Iran and the Khorasan Razavi Regional Water Authority (grant No. 92035-KOW).

References

Ahmadi T, Ziaei AN, Davary K, Faridhosseini A, Izady A (2012) Estimation of groundwater recharge using various methods in Neishaboor Plain, Iran. IAHR International Groundwater Symposium, November 2012, Kuwait

Brunner P, Bauer P, Eugster M, Kinzelbach W (2004) Using remote sensing to regionalize local precipitation recharge rates obtained from the chloride method. J Hydrol 294(4):241–250. https://doi.org/10.1016/j.jhydrol.2004.02.023

Brunner P, Li HT, Kinzelbach W, Li WP, Dong XG (2008) Extracting phreatic evaporation from remotely sensed maps of evapotranspiration. Water Resour Res 44(8). https://doi.org/10.1029/2007wr006063

Brunner P, Doherty J, Simmons CT (2012) Uncertainty assessment and implications for data acquisition in support of integrated hydrologic models. Water Resour Res 48(7). https://doi.org/10.1029/2011wr011342

Cao G (2011) Recharge estimation and sustainability assessment of groundwater resources in the North China Plain. PhD Thesis, The University of Alabama, Tuscaloosa, AL

Cao G, Scanlon BR, Han D, Zheng C (2016) Impacts of thickening unsaturated zone on groundwater recharge in the North China Plain. J Hydrol 537:260–270. https://doi.org/10.1016/j.jhydrol.2016.03.049

Cook PG, Solomon DK (1995) Transport of atmospheric trace gases to the water table: implications for groundwater dating with chlorofluorocarbons and krypton 85. Water Resour Res 31(2):263–270. https://doi.org/10.1029/94wr02232

Corona CR, Gurdak JJ, Dickinson JE, Ferré TPA, Maurer EP (2017) Climate variability and vadose zone controls on damping of transient recharge. J Hydrol. https://doi.org/10.1016/j.jhydrol.2017.08.028

de Vries JJ, Simmers I (2002) Groundwater recharge: an overview of processes and challenges. Hydrogeol J 10(1):5–17. https://doi.org/10.1007/s10040-001-0171-7

Dickinson JE, Ferré TPA, Bakker M, Crompton B (2014) A screening tool for delineating subregions of steady recharge within groundwater models. Vadose Zone J 13(6):15. https://doi.org/10.2136/vzj2013.10.0184

Doherty J (2016) Model-independent Parameter Estimation User Manual Part I: Pest Sensan and Global Optimisers. Watermark Numerical Computing, Brisbane, pp 390

Graham DN, Butts MB (2005) Flexible, integrated watershed modelling with MIKE SHE. In: Watershed models. CRC, Boca Raton, FL

Grismer ME (2013) Estimating agricultural deep drainage lag times to groundwater: application to Antelope Valley, California, USA. Hydrol Process 27(3):378–393. https://doi.org/10.1002/hyp.9249

Harbaugh AW (2005) MODFLOW-2005, the US Geological Survey modular ground-water model: the ground-water flow process. US Geological Survey, Reston, VA

Harrington GA, Cook PG, Herczeg AL (2002) Spatial and temporal variability of ground water recharge in Central Australia: a tracer

approach. Groundwater 40(5):518–527. https://doi.org/10.1111/j.1745-6584.2002.tb02536.x

Healy RW (2010) Estimating groundwater recharge. Cambridge University Press, Cambridge, UK

Hill MC (1998) Methods and guidelines for effective model calibration. US Geological Survey, Denver, CO

Hocking M, Kelly BFJ (2016) Groundwater recharge and time lag measurement through vertosols using impulse response functions. J Hydrol 535:22–35. https://doi.org/10.1016/j.jhydrol.2016.01.042

Horst A, Mahlknecht J, Merkel BJ, Aravena R, Ramos-Arroyo YR (2008) Evaluation of the recharge processes and impacts of irrigation on groundwater using CFCs and radiogenic isotopes in the Silao-Romita basin, Mexico. Hydrogeol J 16(8):1601. https://doi.org/10.1007/s10040-008-0318-x

Hubbell JM, Nicholl MJ, Sisson JB, McElroy DL (2004) Application of a Darcian approach to estimate liquid flux in a deep vadose zone. Vadose Zone J 3(2):560–569. https://doi.org/10.2136/vzj2004.0560

Hunt RJ, Prudic DE, Walker JF, Anderson MP (2008) Importance of unsaturated zone flow for simulating recharge in a humid climate. Groundwater 46(4):551–560. https://doi.org/10.1111/j.1745-6584.2007.00427.x

Izady A, Davary K, Alizadeh A, Ziaei AN, Alipoor A, Joodavi A, Brusseau ML (2014) A framework toward developing a groundwater conceptual model. Arab J Geosci 7(9):3611–3631. https://doi.org/10.1007/s12517-013-0971-9

Izady A, Davary K, Alizadeh A, Ziaei A, Akhavan S, Alipoor A, Joodavi A, Brusseau M (2015) Groundwater conceptualization and modeling using distributed SWAT-based recharge for the semi-arid agricultural Neishaboor plain, Iran. Hydrogeol J 23(1):47–68. https://doi.org/10.1007/s10040-014-1219-9

Khorasan Razavi Regional Water Authority (2011) Final report of extend prohibition of groundwater extraction increase (Neyshaboor plain case study) (in Persian). Ministry of Energy, Mashhad, pp 72

Khorasan-Razavi Regional Water Authority (2010) Water resources study of the Neishaboor watershed report (in Persian). In: Integrated study and water budget, vol 4. Ministry of Energy, Tehran

Kinzelbach W, Aeschbach W, Alberich C, Goni I, Beyerle U, Brunner P, Chiang W, Rueedi J, Zoellmann K (2002) A survey of methods for groundwater recharge in arid and semi-arid regions early warning and assessment report series, United Nations Environment Programme, Nairobi, Kenya

Kinzelbach W, Bauer P, Siegfried T, Brunner P (2003) Sustainable groundwater management: problems and scientific tools. Episodes 2003-news magazine of the International Union of Geological Sciences Ottawa, International Union of Geological Sciences, Paris, pp 279–284

Miller CT, Abhishek C, Farthing MW (2006) A spatially and temporally adaptive solution of Richards' equation. Adv Water Resour 29(4):525–545. https://doi.org/10.1016/j.advwatres.2005.06.008

Nameghi H, Hosseini M, Mb S (2014) An analytical procedure for estimating land subsidence parameters using field data and InSAR images in Nieshaboor plain. J Iran Assoc Eng Geol 6(1–2):33–50

Niswonger RG, Prudic DE, Regan RS (2006) Documentation of the Unsaturated-Zone Flow (UZF1) Package for modeling unsaturated flow between the land surface and the water table with MODFLOW-2005. US Geological Survey, Reston, VA

Niswonger RG, Panday S, Ibaraki M (2011) MODFLOW-NWT, a Newton formulation for MODFLOW-2005. US Geological Survey Techniques and Methods 6-A37

O'Reilly AM (2004) A method for simulating transient ground-water recharge in deep water-table settings in central Florida by using a simple water-balance/transfer-function model. US Geological Survey, Reston, VA

Peel MC, Finlayson BL, McMahon TA (2007) Updated world map of the Köppen-Geiger climate classification. Hydrol Earth Syst Sci 11(5):1633–1644. https://doi.org/10.5194/hess-11-1633-2007

Pfletschinger H, Prömmel K, Schüth C, Herbst M, Engelhardt I (2014) Sensitivity of vadose zone water fluxes to climate shifts in arid settings. Vadose Zone J 13(1):vzj2013.02.0043

Rawls W, Brakensiek D, Saxtonn K (1982) Estimation of soil water properties. Trans ASABE 25(5):1316–1320. https://doi.org/10.13031/2013.33720

Rossman N, Zlotnik VA, Rowe C, Szilagyi J (2014) Vadose zone lag time and potential 21st century climate change effects on spatially distributed groundwater recharge in the semi-arid Nebraska Sand Hills. J Hydrol 519:656–669. https://doi.org/10.1016/j.jhydrol.2014.07.057

Scanlon BR, Healy RW, Cook PG (2002) Choosing appropriate techniques for quantifying groundwater recharge. Hydrogeol J 10(1):18–39. https://doi.org/10.1007/s10040-001-0176-2

Sharma ML, Hughes MW (1985) Groundwater recharge estimation using chloride, deuterium and oxygen-18 profiles in the deep coastal sands of Western Australia. J Hydrol 81(1):93–109. https://doi.org/10.1016/0022-1694(85)90169-6

Singh VP, Joseph ES (1994) Kinematic-wave model for soil-moisture movement with plant-root extraction. Irrig Sci 14(4):189–198. https://doi.org/10.1007/bf00190190

Smith RE (1983) Approximate soil water movement by kinematic characteristics. Soil Sci Soc Am J 47(1):3–8. https://doi.org/10.2136/sssaj1983.03615995004700010001x

Turkeltaub T, Dahan O, Kurtzman D (2014) Investigation of groundwater recharge under agricultural fields using transient deep vadose zone data. Vadose Zone J 13(4). https://doi.org/10.2136/vzj2013.10.0176

Wheater HS, Mathias SA, Li X (2010) Groundwater modelling in arid and semi-arid areas. Cambridge University Press, Cambridge, UK

Zharf Poya (2016) Geoelectric survey in Nieshaboor Plain (in Persian). Khorasan Razavi Regional Water Authority, Mashhad, pp 144